

Ribbon aromaticity in double-chain planar $B_nH_2^{2-}$ and $Li_2B_nH_2$ nanoribbon clusters up to $n = 22$: lithiated boron dihydride analogues of polyenes†

Cite this: *Phys. Chem. Chem. Phys.*, 2013, **15**, 18872

Hui Bai,^a Qiang Chen,^a Chang-Qing Miao,^b Yue-Wen Mu,^a Yan-Bo Wu,^a Hai-Gang Lu,^a Hua-Jin Zhai*^a and Si-Dian Li*^a

We report an extensive density-functional theory and coupled-cluster CCSD(T) study on boron dihydride dianion clusters $B_nH_2^{2-}$ ($n = 6-22$) and their dilithiated $Li_2B_nH_2^{0/-}$ salt complexes. Double-chain (DC) planar nanoribbon structures are confirmed as the global minima for the $B_nH_2^{2-}$ ($n = 6-22$) clusters. Charging proves to be an effective mechanism to stabilize and extend the DC planar nanostructures, capable of producing elongated boron nanoribbons with variable lengths between 4.3–17.0 Å. For the dilithiated salts, the DC planar nanoribbons are lowest in energy up to $Li_2B_{14}H_2$ and represent true minima for all $Li_2B_nH_2^{0/-}$ ($n = 6-22$) species. These boron nanostructures may be viewed as molecular zippers, in which two atomically-thin molecular wires are zipped together *via* delocalized bonds. Bonding analysis reveals the nature of π plus σ double conjugation in the lithiated DC nanoribbon $Li_2B_nH_2^{0/-}$ (n up to 22) model clusters, which exhibit a $4n$ pattern in adiabatic detachment energies, ionization potentials, and second-order differences in total energies. Band structure analysis of the infinite DC boron nanoribbon structure also reveals that both π and σ electrons participate in electric conduction, much different from the monolayer boron α -sheet in which only π electrons act as carriers. A concept of "ribbon aromaticity" is proposed for this quasi-one-dimensional system, where regular π *versus* σ alternation of the delocalized electron clouds along the nanoribbons results in enhanced stability for a series of "magic" nanoribbon clusters. The total number of delocalized π and σ electrons for ribbon aromaticity collectively conforms to the $(4n + 2)$ Hückel rule. Ribbon aromaticity appears to be a general concept in other nanoribbon systems as well.

Received 30th July 2013,
Accepted 10th September 2013

DOI: 10.1039/c3cp53761g

www.rsc.org/pccp

1. Introduction

The structures and chemical bonding of boron have enjoyed a long history of discoveries due to its nature as a prototypical electron-deficient element in the periodic table. It is well known that boron solids consist of icosahedral B_{12} structural units in various polymorphs, whereas boranes favor polyhedral structures in three-dimensional (3D) arrangements. In contrast,

bare boron clusters have been confirmed in recent years to possess planar (2D) or quasi-planar structures^{1–13} up to B_{16}^+ for cations,⁶ B_{20} for neutrals,⁹ and at least B_{23}^- for monoanions.¹³ In 2D boron clusters, the peripheral B atoms are bonded by two-center two-electron (2c–2e) B–B single σ bonds, whereas the inner B atoms interact with one another and with the peripheral atoms *via* delocalized multicenter bonds in order to best compensate boron's electron deficiency. The π bonding patterns of the 2D boron clusters have been shown to closely resemble those of aromatic hydrocarbons.^{1,2} While 2D–3D structural transition is shown to occur at tubular double-ring D_{2d} B_{20} for neutral clusters,⁹ the B_{20}^- anion cluster remains 2D with low symmetry. A recent computational study further reveals the surprising conversion of B_{20} to perfectly planar, circular C_{2v} B_{20}^{2-} dianion upon the attachment of two extra electrons, where the dianion possesses double (or disk) π aromaticity.¹⁴ Obviously, extra electrons are able to introduce dramatic structural changes in boron clusters, offering opportunities to alter or fine-tune their structural, electronic, and bonding properties.

^aInstitute of Molecular Science, Shanxi University, Taiyuan 030006, People's Republic of China. E-mail: hj.zhai@sxu.edu.cn, lisidian@sxu.edu.cn

^bInstitute of Materials Science and Department of Chemistry, Xinzhou Teachers' University, Xinzhou 034000, Shanxi, People's Republic of China

† Electronic supplementary information (ESI) available: Calculated ADEs of $Li_2B_nH_2^-$ monoanions and IPs of $Li_2B_nH_2$ ($n = 6-22$) neutrals at PBE1PBE (Table S1); π CMOs of $Li_2B_nH_2^{0/-}$ ($n = 6-12, 15, 16, 19, \text{ and } 20$) and $B_{20}H_2^{2-}$ as compared with those of C_4H_6 , C_6H_8 , C_8H_{10} , $C_{10}H_{12}$, and $C_{12}H_{14}$ (Fig. S1); σ CMOs of $Li_2B_nH_2^{0/-}$ ($n = 6-12, 15, 16, 19, \text{ and } 20$) and $B_{20}H_2^{2-}$ (Fig. S2); and computational ground-state ADEs of DC planar $B_nH_2^-$ ($n = 4-20$) nanoribbon clusters as a function of n at PBE1PBE/6-311+G(d,p) level, as compared with their experimental values ($n = 7-12$) and those calculated for $B_n(BO)_2^-$ ($n = 4-20$) (Fig. S3). See DOI: 10.1039/c3cp53761g

Partial hydrogenation of 2D bare boron clusters is expected to break the peripheral B–B σ bonds, eventually leading to polyhedral boranes upon increasing hydrogen content. Typical 2D–3D structural transitions have been predicted for $B_{12}H_n^{0/-}$ at around $n = 4$ –5 (ref. 15) and for $B_6H_n^{0/-}$ at $n = 4$.¹⁶ Other hydrogenated boron clusters studied computationally in the literature include the perfectly planar C_{2v} $B_7H_2^-$,¹⁷ D_{3h} $B_{12}H_6$ (the so-called borozene),¹⁸ D_{3h} $B_{18}H_3^-$, D_{2h} $B_{18}H_4$, C_{2v} $B_{18}H_5^+$, and D_{6h} $B_{18}H_6^{2+}$ (the so-called borannulenes),¹⁹ C_{3h} $B_6H_3^+$ and C_{2h} B_8H_2 ,²⁰ quasi-2D $B_{16}H_6$,²¹ and the dicyclic aromatic $B_{30}H_8$ and $B_{26}H_8$.^{22,23} Remarkably, recent photoelectron spectroscopy (PES) and quantum chemical calculations have shown that boron dihydride clusters, $B_nH_2^{0/-}$ ($n = 3$ –12), possess elongated double-chain (DC) planar nanoribbon structures, analogous to polyenes in terms of π conjugation.^{24,25} However, such nanoribbon structures stop at $n = 12$ for B_nH_2 . A quasi-planar C_s $B_{12}H_2$ structure appears to be the global minimum,²⁴ which is based on the experimentally observed convex C_{3v} B_{12} cluster.⁸ It is thus of interest and importance to ask at this stage if it is possible, and how, to further extend the DC planar nanoribbon clusters to even longer sizes, which are analogues of larger polyenes. In the current contribution, we aim to explore a “design” strategy computationally and address the above question.

We report herein on a density-functional theory (DFT) and coupled-cluster with single, double, and perturbative triple excitations [CCSD(T)] study on the doubly-charged $B_nH_2^{2-}$ ($n = 6$ –22) clusters and their lithiation. All dihydride dianion DC planar $B_nH_2^{2-}$ ($n = 6$ –22) nanoribbon clusters are confirmed as the global minima, while the dilithiated $Li_2B_nH_2^{0/-}$ salt complexes are the global minimum structures up to $n = 14$. The $B_nH_2^{2-}$ ($n = 6$ –22) clusters significantly extend the DC planar molecular nanoribbons to up to 17.0 Å in length, as compared to a limit of 11.1 Å in the $B_nH_2^{0/-}$ series.^{24,25} These nanoribbon clusters can be considered as interesting molecular zippers, where two molecular wires are held together by delocalized bonds. To explore the properties of these quasi-one-dimensional (quasi-1D) clusters, we analyzed the chemical bonding of the $Li_2B_nH_2^{0/-}$ ($n = 6$ –22) DC nanoribbons, among which those for $n > 14$ should be considered as model clusters. Canonical molecular orbital (CMO), adaptive natural density partitioning (AdNDP),²⁶ electron localization function (ELF),^{27–29} and nucleus independent chemical shift (NICS)³⁰ analyses show that these molecular ribbons are overall aromatic in nature with unique π plus σ double conjugation. The DC nanoribbon $Li_2B_nH_2^{0/-}$ ($n = 6$ –22) are lithiated boron dihydride analogues of the polyenes. We propose here a new concept of “ribbon aromaticity” to account for the high stability of a series of magic $B_nH_2^{0/-/2-}$ and $Li_2B_nH_2^{0/-}$ clusters, which possess $2(n + 1)$ delocalized π electrons and $2n$ delocalized σ electrons, whose total counting collectively conforming to the $(4n + 2)$ Hückel rule. The underlying mechanism for ribbon aromaticity and its electron counting rule is addressed. This work shows that charging can be a means to extend and stabilize the elongated DC planar nanoribbon structures, which may find applications in the design and fabrications of boron nanomaterials.

2. Computational methods

Structural optimizations and frequency analyses were carried out at the PBE1PBE level^{31–33} with complementary calculations at B3LYP,^{34,35} using the 6-311+G(d,p) basis sets as implemented in Gaussian 09 program.³⁶ Benchmarking using single-point CCSD(T) calculations^{37–39} with the same bases for $B_{14}H_2^{2-}$ and $B_{18}H_2^{2-}$ clusters indicates that the energetics from PBE1PBE is in quantitative agreement with CCSD(T) for the current B–H systems, whereas that from B3LYP deviate substantially from CCSD(T). Thus, PBE1PBE is chosen as the primary method throughout the current work.

Global-minimum searches were performed for the $B_nH_2^{2-}$ ($n = 6, 10, 14, 18,$ and 22) binary clusters *via* the Basin-Hopping procedure.^{22,40} Additionally, initial structures were also constructed based upon the low-lying isomers of bare $B_n^{0/-/2-}$ clusters reported in the literature. Low-lying isomers of ternary $Li_2B_nH_2$ ($n = 6, 10, 14,$ and 18) clusters were obtained based upon $B_nH_2^{2-}$ by placing two Li atoms around the DC planar frame at different positions. Subsequently, whole series of DC planar $B_nH_2^{2-}$ and $Li_2B_nH_2^{0/-}$ ($n = 6$ –22) nanoribbon clusters were fully optimized, at both PBE1PBE and B3LYP levels. The CMO, AdNDP, ELF, and NICS analyses were performed to elucidate the bonding patterns of the clusters. The ELF_σ and ELF_π bifurcation values were approximated using the Molekel 5.4 software.⁴¹

3. Results and discussion

3.1. DC planar $B_{14}H_2^{2-}$, $B_{18}H_2^{2-}$, and $B_{22}H_2^{2-}$ nanoribbon dianions and their dilithiated $Li_2B_nH_2$ salts

To explore the DC planar nanoribbon structures beyond the B_{12} cluster, we start from the $B_{14}H_2^{2-}$ and $B_{18}H_2^{2-}$ dianions, which are the dihydrogenated products of quasi-planar C_{2v} B_{14}^- and convex C_{3v} B_{18}^- .^{8,12} These dianion species are anticipated to possess the same number of delocalized electrons as the corresponding $B_{4n}H_2$ clusters,^{24,25} due to the fact that each B atom contributes effectively one delocalized electron in the DC planar nanoribbons. The optimized structures and energetics for $B_{14}H_2^{2-}$ and $B_{18}H_2^{2-}$ are shown in Fig. 1. All PBE1PBE, B3LYP, and single-point CCSD(T) calculations concurred indicate that the elongated DC planar nanoribbon structures are the global minima for $B_{14}H_2^{2-}$ and $B_{18}H_2^{2-}$, which lie at least ~ 17 and ~ 14 kcal mol⁻¹ lower than alternative structures, respectively. Thus, although the DC planar nanoribbon structures terminate at $n = 12$ for $B_nH_2^{0/-}$,^{24,25} charging provides a heretofore unexplored mechanism to elongate large $B_nH_2^{2-}$ clusters beyond $n > 12$. In terms of the energetics, the PBE1PBE data are remarkably close to those at CCSD(T), whereas the B3LYP data deviate substantially from CCSD(T). The data set in Fig. 1a and b serves as a valuable and reliable benchmark for the computational methods, suggesting that PBE1PBE performs superior for the B–H systems and should be the method of choice throughout the current work, which can effectively reduce the computational cost relative to CCSD(T) calculations.

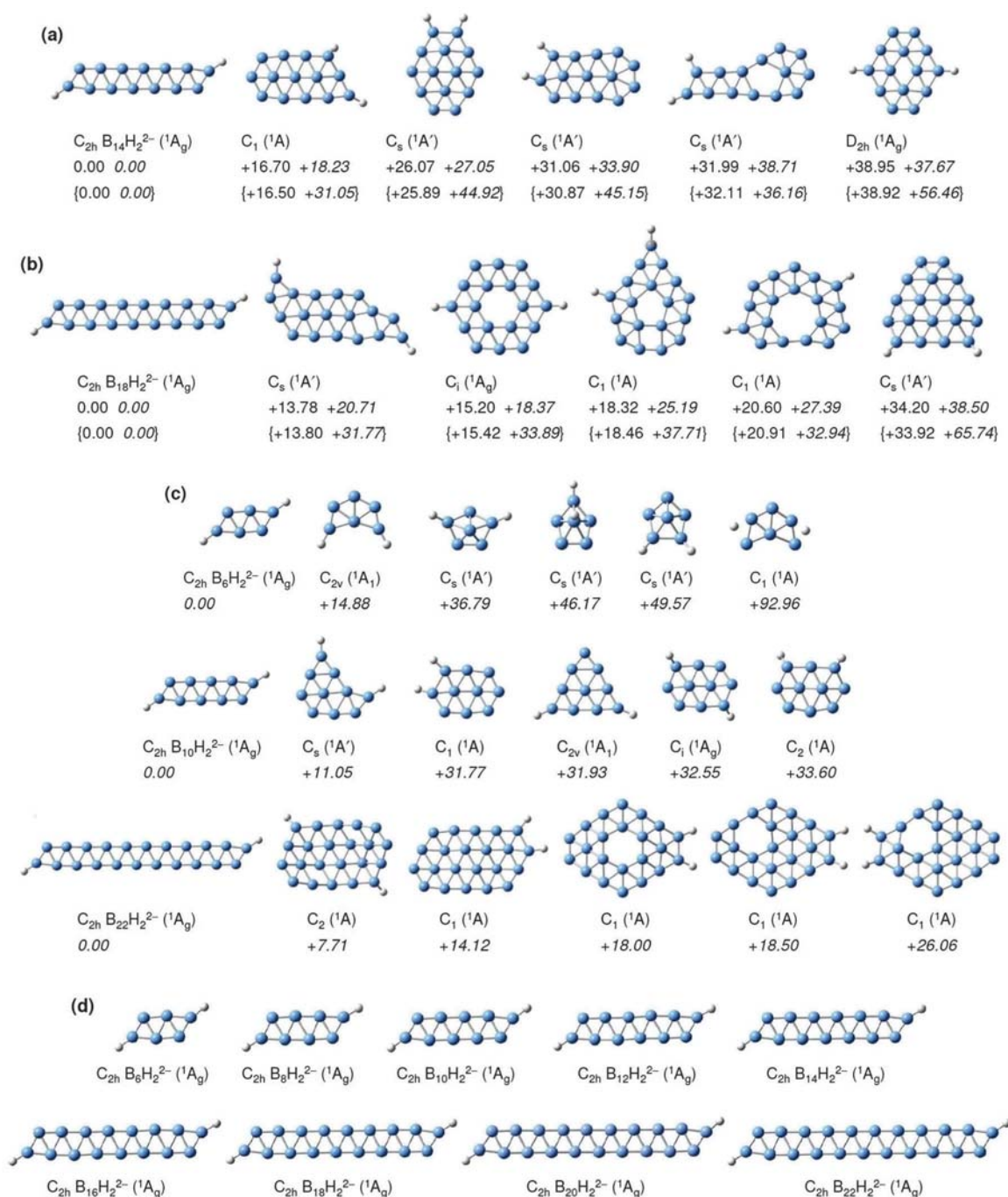


Fig. 1 Optimized structures at the PBE1PBE level for (a) $B_{14}H_2^{2-}$, (b) $B_{18}H_2^{2-}$, (c) $B_6H_2^{2-}$, $B_{10}H_2^{2-}$, and $B_{22}H_2^{2-}$, and (d) the series of DC planar nanoribbon global minima of $B_nH_2^{2-}$ ($n = 6, 8, 10, 12, 14, 16, 18, 20$, and 22) clusters. Relative energies are labeled in kcal mol $^{-1}$ at CCSD(T)//PBE1PBE, PBE1PBE (*italic*), CCSD(T)//B3LYP (in curly brackets), and B3LYP (*italic* in curly brackets). Boron is in blue, and H in gray.

To further explore the larger DC planar nanoribbon $B_nH_2^{2-}$ clusters, we carried out structural searches for $B_{22}H_2^{2-}$, that is, the dihydrogenated species of quasi-planar B_{22}^- .¹³ The PBE1PBE energetics shows that DC planar nanoribbon $B_{22}H_2^{2-}$ is ~ 8 kcal mol $^{-1}$ more stable than the nearest alternative isomer (Fig. 1c). Thus, the DC planar nanoribbon can be safely claimed as the global minimum for $B_{22}H_2^{2-}$ as well, extending such nanostructures to up to 17.0 Å in length.

Even larger DC planar nanoribbon clusters, $B_nH_2^{2-}$ ($n > 22$), are possible and the ultimate upper-limit size is still open. However, a global search for such large binary clusters is computationally too costly for us to pursue at present.

For smaller dianion $B_nH_2^{2-}$ ($n < 12$) clusters, DC planar nanoribbon structures should prevail as their global minima, as exemplified by $B_6H_2^{2-}$ and $B_{10}H_2^{2-}$ (Fig. 1c). This is so for two reasons. First, recent experimental and theoretical

studies^{24,25} have established the DC planar nanoribbon structures as the global minima for neutral and monoanion $B_nH_2^{0/-}$ clusters in this size range. Second, the intramolecular coulomb repulsion provides an additional driving force to stabilize the elongated DC planar structures for small $B_nH_2^{2-}$ dianion clusters. In summary, the above results lead us to conclude that all $B_nH_2^{2-}$ ($n \leq 22$) dianion clusters adopt the DC planar nanoribbon structures as the global minima, a subset of which are depicted in Fig. 1d.

As the $B_nH_2^{2-}$ ($n = 6-22$) dianion clusters are unstable towards electron autodetachment, their dilithiated $Li_2B_nH_2^{0/-}$ salts are pursued, where $B_nH_2^{2-}$ are effectively stabilized by incorporation of two Li^+ counter-ions. Systematic global-minimum searches for $Li_2B_nH_2^{0/-}$ ternary series are too computationally demanding to be implemented, we have thus chosen to evaluate the structures of $Li_2B_{14}H_2$ and $Li_2B_{18}H_2$ (Fig. 2) on the basis of those of $B_{14}H_2^{2-}$ and $B_{18}H_2^{2-}$ (Fig. 1) by attaching the Li atoms in various possible sites. The PBE1PBE energetics indicates that the DC planar nanoribbon structure is the global minimum for $Li_2B_{14}H_2$ (Fig. 2a), whereas a more circular structure with a hexagonal hole at the center is found for $Li_2B_{18}H_2$, with the DC planar nanoribbon being a low-lying isomer (Fig. 2b). Thus, lithiation results in a shift of the upper-limit size of the DC planar

nanoribbon structures in $Li_2B_nH_2$ to around $n = 14$, as compared to up to $n = 22$ in $B_nH_2^{2-}$, further highlighting that charging is an effective mechanism to stabilize the nanoribbon structures. This observation may be rationalized considering that the two Li^+ counter-ions can effectively quench the intramolecular coulomb repulsion in $B_nH_2^{2-}$ units, resulting in neutral $Li_2B_nH_2$ salt complexes where coulomb repulsion no longer plays a dominant role. It is commented that the DC nanoribbon $B_nH_2^{2-}$ dianion structures, while unstable in the gas phase towards autodetachment, may be stabilized on surface or in nanofabrication processes *via* charging.

As model systems, the closed-shell C_{2h} $Li_2B_nH_2$ ($n =$ even integers) neutrals (Fig. 2c) and C_{2v} $Li_2B_nH_2^-$ monoanions ($n =$ odd integers) (Fig. 2d) possess perfectly planar DC *trans* and *cis* nanoribbon structures, respectively. These can be faithfully formulated as $[Li(HB_nH)Li]^{0/-}$ with a B_n core, which all prove to be true minima on their potential energy surfaces.

3.2. Double (π plus σ) conjugation in DC planar $Li_2B_nH_2$ and $B_nH_2^{2-}$ nanoribbon clusters

The DC planar nanoribbon $Li_2B_nH_2^{0/-}$ ($n = 6-22$) clusters present a valuable model system for chemical bonding analyses. As revealed from the CMOs (Fig. 3 and Fig. S1 in ESI[†]),

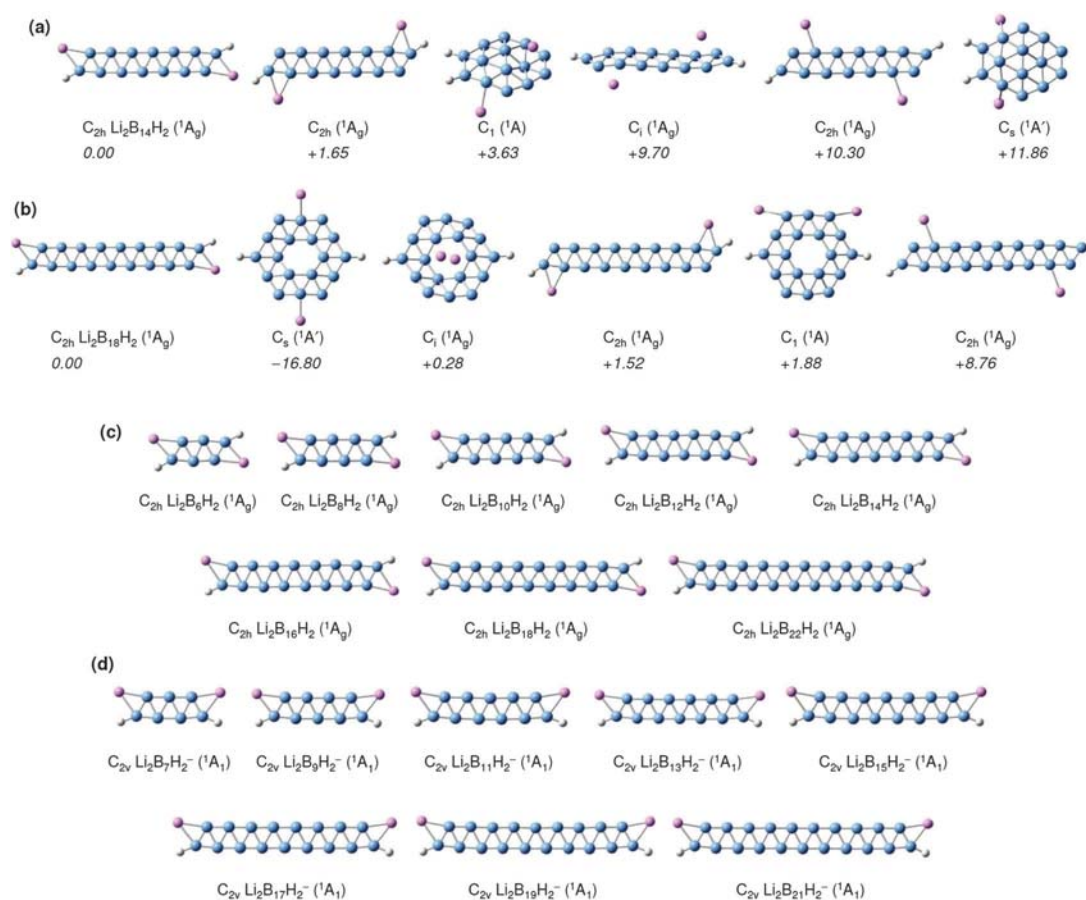


Fig. 2 Optimized structures of (a) $Li_2B_{14}H_2$, (b) $Li_2B_{18}H_2$, and the series of DC planar (c) *trans* C_{2h} and (d) *cis* C_{2v} nanoribbon structures of $Li_2B_nH_2^{0/-}$ ($n = 6-22$) clusters at the PBE1PBE level. All nanoribbon structures in (c) and (d) are true minima and those for $n = 6-14$ are global minima. Relative energies are labeled in kcal mol⁻¹ in (a) and (b). Boron is in blue, H in gray, and Li in purple.

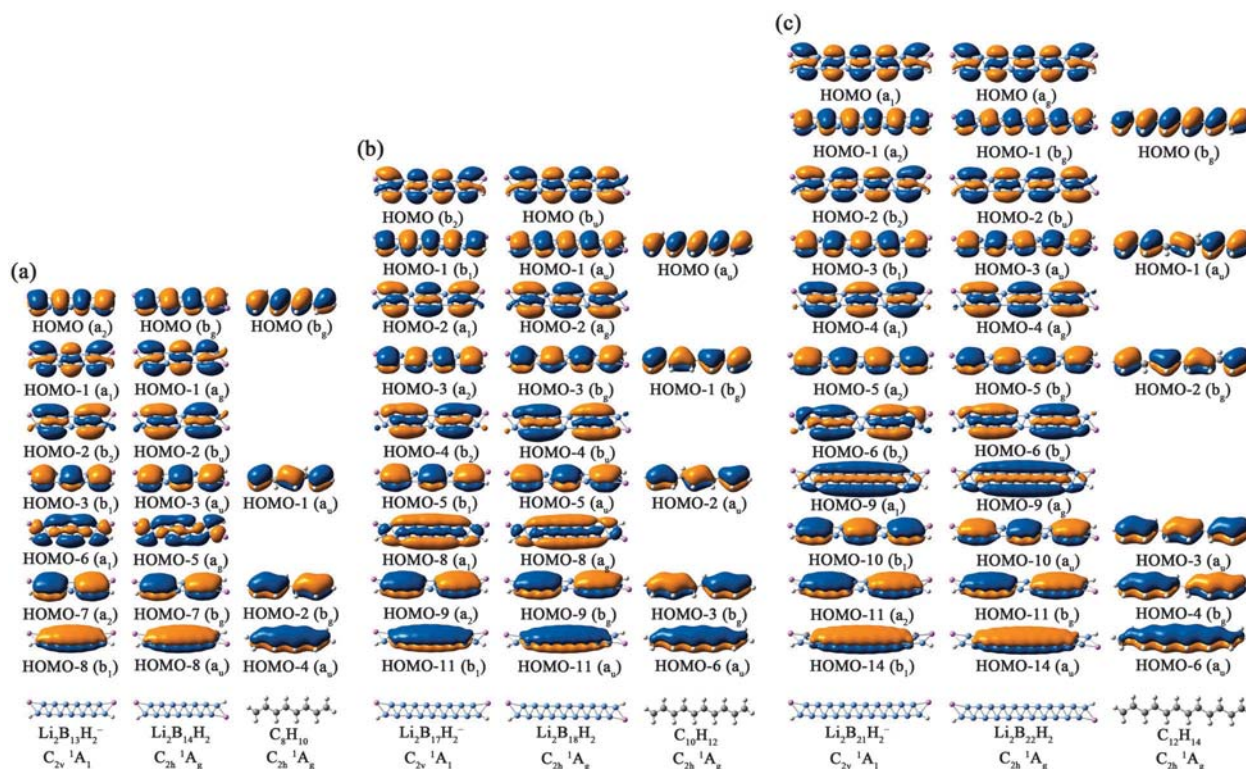


Fig. 3 Delocalized π and σ CMOs of (a) $\text{Li}_2\text{B}_{13}\text{H}_2^-$ and $\text{Li}_2\text{B}_{14}\text{H}_2$, (b) $\text{Li}_2\text{B}_{17}\text{H}_2^-$ and $\text{Li}_2\text{B}_{18}\text{H}_2$, and (c) $\text{Li}_2\text{B}_{21}\text{H}_2^-$ and $\text{Li}_2\text{B}_{22}\text{H}_2$, as compared with the delocalized π CMOs of C_8H_{10} , $\text{C}_{10}\text{H}_{12}$, and $\text{C}_{12}\text{H}_{14}$, respectively. Note that C_nH_{n+2} polyenes possess no delocalized σ framework.

the $\text{Li}_2\text{B}_6\text{H}_2/\text{Li}_2\text{B}_7\text{H}_2^-/\text{Li}_2\text{B}_8\text{H}_2$, $\text{Li}_2\text{B}_9\text{H}_2^-/\text{Li}_2\text{B}_{10}\text{H}_2/\text{Li}_2\text{B}_{11}\text{H}_2^-/\text{Li}_2\text{B}_{12}\text{H}_2$, and $\text{Li}_2\text{B}_{13}\text{H}_2^-/\text{Li}_2\text{B}_{14}\text{H}_2/\text{Li}_2\text{B}_{15}\text{H}_2^-/\text{Li}_2\text{B}_{16}\text{H}_2$ groups of species each have two, three, and four delocalized π CMOs, analogous to the π -conjugated 1,3-butadiene C_{2h} C_4H_6 , 1,3,5-hexatriene C_{2h} C_6H_8 , and 1,3,5,7-octotetraene C_{2h} C_8H_{10} , respectively. Similarly, the $\text{Li}_2\text{B}_{17}\text{H}_2^-/\text{Li}_2\text{B}_{18}\text{H}_2/\text{Li}_2\text{B}_{19}\text{H}_2^-$ and $\text{Li}_2\text{B}_{20}\text{H}_2/\text{Li}_2\text{B}_{21}\text{H}_2^-/\text{Li}_2\text{B}_{22}\text{H}_2$ groups of species have five and six delocalized π CMOs, respectively, which are analogues of C_{2h} $\text{C}_{10}\text{H}_{12}$ and C_{2h} $\text{C}_{12}\text{H}_{14}$. In short, the $\text{Li}_2\text{B}_n\text{H}_2^{0/-}$ clusters can be viewed as the lithiated boron dihydride analogues to polyenes in terms of π bonding.

Further analyses show that $\text{Li}_2\text{B}_6\text{H}_2$ also possesses one delocalized σ CMO, whereas the $\text{Li}_2\text{B}_7\text{H}_2^-/\text{Li}_2\text{B}_8\text{H}_2/\text{Li}_2\text{B}_9\text{H}_2^-/\text{Li}_2\text{B}_{10}\text{H}_2$, $\text{Li}_2\text{B}_{11}\text{H}_2^-/\text{Li}_2\text{B}_{12}\text{H}_2/\text{Li}_2\text{B}_{13}\text{H}_2^-/\text{Li}_2\text{B}_{14}\text{H}_2$, $\text{Li}_2\text{B}_{15}\text{H}_2^-/\text{Li}_2\text{B}_{16}\text{H}_2/\text{Li}_2\text{B}_{17}\text{H}_2^-/\text{Li}_2\text{B}_{18}\text{H}_2/\text{Li}_2\text{B}_{20}\text{H}_2$, and $\text{Li}_2\text{B}_{19}\text{H}_2^-/\text{Li}_2\text{B}_{21}\text{H}_2^-/\text{Li}_2\text{B}_{22}\text{H}_2$ groups of clusters each have two, three, four, and five delocalized σ CMOs, respectively (Fig. 3 and Fig. S2 in ESI†). It is stressed that classical polyenes have no delocalized multicenter σ CMOs, and they possess solely delocalized π CMOs that are composed of C $2p_z$ contributions (Fig. 3). This marks the major difference in bonding between polyboroenes and polyenes. Indeed, all $\text{Li}_2\text{B}_n\text{H}_2^{0/-}$ clusters possess unique π plus σ double conjugation, whose σ and π components are independent with each other and play equally critical roles in defining the bonding nature of the system. The same bonding patterns are true for the $\text{B}_n\text{H}_2^{2-}$ ($n = 6-22$) dianion clusters, for which that of $\text{B}_{20}\text{H}_2^{2-}$ is depicted as an example (Fig. S1 and S2 in ESI†). We note that π plus σ double conjugation exists, but was not

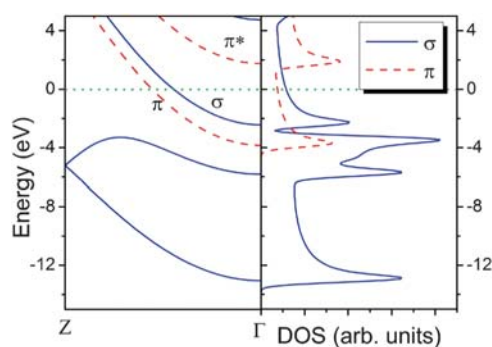


Fig. 4 Band structure and density of states (DOS) of an infinite double-chain boron nanoribbon. The Gaussian broadening is 0.5 eV full width at half maximum (FWHM) and the Fermi energy is set to zero.

previously recognized, in the $\text{B}_n\text{H}_2^{0/-}$ ($n = 3-12$) systems.^{24,25} Relevant π and σ double delocalization was first discussed in the dicyclic C_{2h} B_{30}H_8 molecular sheet, in which the electron clouds are distributed circularly.²²

It is interesting to examine the band structure of an infinite DC planar boron nanoribbon.⁴²⁻⁴⁴ As shown in Fig. 4, a σ band and a π band cross the Fermi level, indicating that the DC boron ribbon is metallic in nature in σ and π bonding. Thus both σ and π electrons act as carriers for conductivity in the infinite DC planar boron nanoribbon, in line with π plus σ double conjugation in the shorter DC nanoribbon clusters. This situation is much different from the 2D monolayer boron α -sheet, where only π electrons participate in electric conductance.⁴⁵ The π and σ bands are both nearly

half-filled, with the density of state (DOS) of the σ band being larger at Fermi level than the π band, implying that σ electrons actually contribute more to the conductivity than π electrons.

3.3. The $4n$ pattern in electron affinities and ionization potentials of $\text{Li}_2\text{B}_n\text{H}_2$

The calculated electron affinities (EAs) of the DC planar $\text{Li}_2\text{B}_n\text{H}_2$ nanoribbon neutrals, that is, the adiabatic detachment energies (ADEs) of the $\text{Li}_2\text{B}_n\text{H}_2^-$ monoanions, are depicted in Fig. 5a and listed in Table S1 in the ESI.† Shown in Fig. 5b are the ionization potentials (IPs) of these neutral clusters. The ADEs of $\text{Li}_2\text{B}_n\text{H}_2^-$ exhibit a $4n$ pattern *versus* cluster size, which reach their “magic” maxima at $n = 9, 13, 17,$ and 21 and their minima at $n = 10, 14, 18,$ and 22 , in a periodicity of every four B atoms. Such a pattern divides the $\text{Li}_2\text{B}_n\text{H}_2^-$ monoanions into four “periods”: $n = 6-9, 10-13, 14-17,$ and $18-21$. The magic $\text{Li}_2\text{B}_n\text{H}_2^-$ monoanions possess closed-shell electron configurations of $\pi^6\sigma^4, \pi^8\sigma^6, \pi^{10}\sigma^8,$ and $\pi^{12}\sigma^{10}$, respectively (Fig. 5a), whereas those at the minima have open-shell configurations with one extra electron in their singly occupied HOMOs (SOMOs), that is, the LUMOs of $\text{Li}_2\text{B}_n\text{H}_2$ neutrals.

A similar but more obvious $4n$ periodicity is observed in the IPs of $\text{Li}_2\text{B}_n\text{H}_2$ neutral clusters (Fig. 5b), which reach their magic maxima at $n = 6, 10, 14, 18,$ and 22 , and minima at $n = 7, 11, 15,$ and 19 . The magic $\text{Li}_2\text{B}_n\text{H}_2$ neutrals have the closed-shell configurations of $\pi^4\sigma^2, \pi^6\sigma^4, \pi^8\sigma^6, \pi^{10}\sigma^8,$ and

$\pi^{12}\sigma^{10}$, respectively, identical to those magic clusters in the ADEs. Their open-shell $\text{Li}_2\text{B}_{n+1}\text{H}_2$ nearest neighbors, with one more delocalized electron, have the lowest IPs as anticipated. Note that the ADEs of $\text{Li}_2\text{B}_n\text{H}_2^-$ monoanions reach their maxima one B atom earlier than the IPs of $\text{Li}_2\text{B}_n\text{H}_2$ neutrals, for the reason that the monoanions carry one more delocalized electron (either π or σ) than their neutrals. Thus, the magic clusters are entirely due to electronic rather than structural effects. We also notice that the minimum ADEs of $\text{Li}_2\text{B}_n\text{H}_2^-$ increase almost linearly with cluster size, and the minimum IPs of $\text{Li}_2\text{B}_n\text{H}_2$ decrease linearly (Fig. 5), hinting that the stabilities of the DC planar $\text{Li}_2\text{B}_n\text{H}_2$ neutrals deteriorate gradually with ribbon length.

The series of magic clusters in $\text{Li}_2\text{B}_n\text{H}_2^{0/-}$ ($n = 6-22$) may also be characterized using an energetic criterion,⁴⁶ that is, the second-order difference in total energies: $\Delta_2(E_n) = E_{n+1} + E_{n-1} - 2E_n$, where E_n is the total energy of a specific $\text{Li}_2\text{B}_n\text{H}_2^{0/-}$ cluster. This criterion approaches a magic cluster *via* its enhanced energetic stability relative to its nearest neighbors. The $\Delta_2(E_n)$ values show maxima at $n = 9, 13, 17,$ and 21 for $\text{Li}_2\text{B}_n\text{H}_2^-$ (Fig. 5c) and $n = 10, 14, 18,$ and 22 for $\text{Li}_2\text{B}_n\text{H}_2$ (Fig. 5d), in complete consistency with the magic numbers observed in ADEs and IPs, respectively.

3.4. Ribbon aromaticity and its $(4n + 2)$ electron counting rule

Aromaticity has remained one of the most popular, and sometimes controversial, concepts in chemistry. Various evaluation

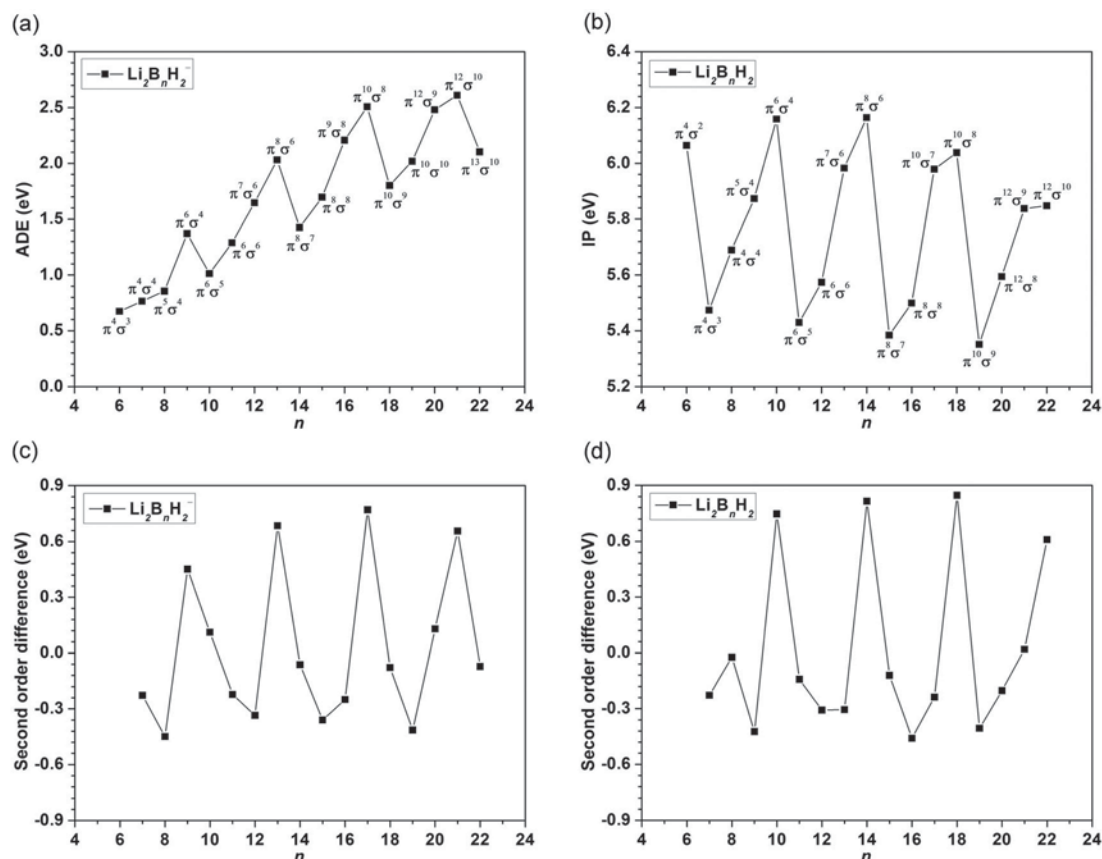


Fig. 5 Calculated curves as a function of size n at the PBE1PBE level for (a) ADEs of DC planar $\text{Li}_2\text{B}_n\text{H}_2^-$ ($n = 6-22$) clusters, (b) IPs of $\text{Li}_2\text{B}_n\text{H}_2$ ($n = 6-22$), and second-order difference in total energy (Δ_2E) of (c) $\text{Li}_2\text{B}_n\text{H}_2^-$ ($n = 7-22$) and (d) $\text{Li}_2\text{B}_n\text{H}_2$ ($n = 7-22$). Electron configurations are labeled in (a) and (b).

criteria, including the $(4n + 2)$ Hückel rule, resonance energy, ELF, and NICS, have been used to assess the overall and local aromaticity. In this work, we chose to use ELF and the perpendicular component of NICS (NICS_{zz}) to evaluate aromaticity in the magic DC planar $\text{Li}_2\text{B}_n\text{H}_2^{0/-}$ nanoribbon clusters. Santos and coworkers²⁹ have established from various organic and inorganic systems that aromatic molecules possess the average bifurcation values of ELF_{av} [$\text{ELF}_{\text{av}} = (\text{ELF}_{\sigma} + \text{ELF}_{\pi})/2$] greater than 0.70 on the interval of (0, 1). As tabulated in Table 1, all the magic DC planar $\text{Li}_2\text{B}_n\text{H}_2^{0/-}$ clusters possess the bifurcation values of $\text{ELF}_{\sigma} = 0.83$ – 0.84 , $\text{ELF}_{\pi} = 0.65$ – 0.83 , and their averages of $\text{ELF}_{\text{av}} = 0.74$ – 0.83 . Thus, these DC planar dilithiated polyboroenes are all overall aromatic in nature on the basis of the ELF criterion. Note that these $\text{Li}_2\text{B}_n\text{H}_2^{0/-}$ clusters possess similar ELF values and AdNDP bonding patterns, in which the electron delocalization forms both π and σ aromatic islands along the nanoribbons. The island aromaticity is also supported by the calculated negative $\text{NICS}_{zz}(0)$ values between -39.6 and -44.5 ppm at the center of each delocalized σ bond and the negative $\text{NICS}_{zz}(1)$ values between -6.8

and -18.9 ppm at 1.0 \AA above the center of each delocalized π bond.

To elucidate the unusual high stability of the magic DC planar $\text{Li}_2\text{B}_n\text{H}_2^{0/-}$ clusters with maximum ADEs and IPs in the $4n$ pattern (Fig. 5), we propose here a new kind of aromaticity, that is, “ribbon aromaticity”. The ribbon aromatic clusters share the common electron configuration of $\pi^{2(n+1)}\sigma^{2n}$ (Fig. 5), with $(n + 1)$ delocalized π bonding CMOs and n delocalized σ bonding CMOs. Consequently, the total number of delocalized electrons amounts to $2(n + 1)\pi + 2n\sigma$, that is, $(4n + 2)$, which is exactly the Hückel rule. It is justified to count the delocalized π and σ electrons together in the DC planar nanoribbon clusters on the ground that: (i) all delocalized σ and π CMOs in the DC nanoribbons originate from the overlaps (in “ π ” fashion) between B 2p atomic orbitals (AOs) of neighboring atoms in the single B chains. Only after the two single chains are combined into nanoribbons do these “ π ” orbitals from the single B chains couple into either π or σ CMOs of the DC planar clusters. In short, the π and σ CMOs in the DC planar clusters have the same origin as “ π ” orbitals of

Table 1 The ELF and AdNDP bonding patterns of DC planar nanoribbon C_{2h} $\text{Li}_2\text{B}_n\text{H}_2$ ($n = 6, 10, 14, 18,$ and 22) neutral clusters. Approximated bifurcation values of ELF_{σ} , ELF_{π} , and their averages ELF_{av} , are also tabulated. $\text{NICS}_{zz}(0)$ values are calculated at the center of each delocalized σ -bond and $\text{NICS}_{zz}(1)$ values at 1.0 \AA above the center of each delocalized π -bond

Structure		ELF_{σ}	ELF_{π}	ELF_{av}
 $\text{C}_{2h} \text{Li}_2\text{B}_6\text{H}_2 ({}^1A_g)$	ELF	0.83	0.65	0.74
	AdNDP			
	NICS	$-44.3(\text{b})$	$-11.7(\text{a})$	
 $\text{C}_{2h} \text{Li}_2\text{B}_{10}\text{H}_2 ({}^1A_g)$	ELF	0.84	0.76	0.80
	AdNDP			
	NICS	$-44.0(\text{d})$	$-13.6(\text{c})$ $-6.8(\text{e})$	
 $\text{C}_{2h} \text{Li}_2\text{B}_{14}\text{H}_2 ({}^1A_g)$	ELF	0.84	0.81	0.83
	AdNDP			
	NICS	$-44.1(\text{g})$ $-40.7(\text{i})$	$-16.2(\text{f})$ $-9.5(\text{h})$	
 $\text{C}_{2h} \text{Li}_2\text{B}_{18}\text{H}_2 ({}^1A_g)$	ELF	0.84	0.82	0.83
	AdNDP			
	NICS	$-44.3(\text{k})$ $-40.4(\text{m})$	$-17.8(\text{j})$ $-10.2(\text{l})$ $-11.6(\text{n})$	
 $\text{C}_{2h} \text{Li}_2\text{B}_{22}\text{H}_2 ({}^1A_g)$	ELF	0.83	0.83	0.83
	AdNDP			
	NICS	$-44.5(\text{p})$ $-40.3(\text{r})$ $-39.6(\text{t})$	$-18.9(\text{o})$ $-10.7(\text{q})$ $-12.2(\text{s})$	

the single B chains. Based on this understanding, the DC planar boron nanoribbons are exact model molecular zippers, in which two atomic B wires are zipped together *via* the unique bonding of ribbon aromaticity. (ii) The delocalized π and σ CMOs are highly mixed in sequence based on their energies, into which the available valence electrons in the system successively fill. Indeed, in the growth of nanoribbon $\text{Li}_2\text{B}_n\text{H}_2^{0/-}$ clusters, each newcomer B atom brings in one extra delocalized electron,⁴⁷ whose identity as π or σ in the CMOs is sensitively size dependent. Normally, when two electrons occupy a π CMO, the next two would fill in a σ CMO. Thus, delocalized π or σ electrons are routinely equivalent and indistinguishable in the system. It is not surprising that they are counted together to assess the overall stability of the nanoribbons.

The $(4n + 2)$ counting in the DC planar nanoribbons may be conveniently achieved either by an appropriate number of boron atoms, or by charging, or both. One consequence of $(4n + 2)$ electrons is to produce a unique bonding pattern, in which the π *versus* σ clouds alternate regularly along the ribbons as revealed from the AdNDP analyses (Table 1). In such magic clusters, the electron clouds distribute nearly evenly on each segment of the nanoribbons, which, while maintaining the optimal delocalized π or σ bonding within the B_3/B_4 units, should effectively reduce the intramolecular electrostatic repulsion in the system. This appears to be the key mechanism that underlie the ribbon aromaticity and its $(4n + 2)$ rule.

For $\text{B}_n\text{H}_2^{2-}$ dianion clusters, the extra charges offer a further driving force for their structural elongation in order to minimize the coulomb repulsion between the extra charges, thus extending the nanoribbon structures to larger sizes up to $n = 22$ for $\text{B}_n\text{H}_2^{2-}$ as compared to $n = 12$ for B_nH_2 clusters.^{24,25} The DC planar nanostructures are the narrowest molecular ribbons to achieve ribbon aromaticity. It is expected that ribbon aromaticity may exist in a wide range of nanoribbon molecules with conjugated π and σ CMOs, such as the previous B_nH_2^- clusters^{24,25} and their isovalent boron boronyl $\text{B}_n(\text{BO})_2^-$ complexes (see Fig. S3 in ESI†). Monolayer boron sheets^{22,46,48–50} of recent interest may also have ribbon aromatic characters, which warrant further theoretical studies. Lastly, it is noted that the quasi-1D boron nanoribbons are critical building blocks in a variety of low-dimensional boron nanostructures, including tubular B_n clusters,^{6,9} B_{80} fullerene,⁵¹ boron nanotubes,⁵² and 2D interwoven boron sheets. Similar nanostructures are also likely to exist as extended or zigzag substructures in Li_mB_n binary solids, which are promising cathode materials in environment friendly Li-ion batteries.

4. Conclusions

Based upon PBE1PBE and CCSD(T) calculations, we show that the $\text{B}_n\text{H}_2^{2-}$ dianion clusters adopt elongated double-chain planar nanoribbon structures up to $n = 22$, whereas similar structures are stable for their dilithiated $\text{Li}_2\text{B}_n\text{H}_2^{0/-}$ salt clusters up to $n = 14$. These nanostructures serve as interesting models for molecular zippers. Charging thus provides a valuable mechanism to stabilize these elongated boron nanostructures,

up to 17.0 Å in length for $\text{B}_n\text{H}_2^{2-}$. The $\text{Li}_2\text{B}_n\text{H}_2^{0/-}$ nanoribbon clusters are boron-based analogues of polyenes, which prove to be overall aromatic in nature with π plus σ double conjugation. The calculated electron affinities and ionization potentials of $\text{Li}_2\text{B}_n\text{H}_2$ both exhibit a $4n$ pattern with cluster size, featuring a series of magic numbers: $n = 9, 13, 17,$ and 21 in electron affinities and $n = 10, 14, 18,$ and 22 in ionization potentials. The same sets of magic clusters are revealed in the second-order difference in total energies. We propose a new concept, “ribbon aromaticity”, to account for these magic clusters, extending aromaticity from 2D, 3D, to quasi-1D. In ribbon aromaticity, a double-chain planar nanoribbon cluster with the electron configuration of $\pi^{2(n+1)}\sigma^{2n}$ shows enhanced stability, which possesses $(4n + 2)$ delocalized π and σ electrons in total, formally conforming to the Hückel rule. The $(4n + 2)$ electrons show a regular spatial π *versus* σ alternation along the nanoribbons, resulting in evenly distributed electron clouds and reduced electrostatic repulsion in the system. This rationalizes the observations of enhanced stability, magic nanoribbon clusters, and ribbon aromaticity. Ribbon aromaticity may exist in other nanoribbon systems as well.

Acknowledgements

This work was supported by the National Natural Science Foundation of China (No. 21243004 and 21373130). H.J.Z. gratefully acknowledges the start-up fund from Shanxi University for support.

References

- 1 A. N. Alexandrova, A. I. Boldyrev, H. J. Zhai and L. S. Wang, *Coord. Chem. Rev.*, 2006, **250**, 2811–2866.
- 2 D. Yu. Zubarev and A. I. Boldyrev, *J. Comput. Chem.*, 2007, **28**, 251–268.
- 3 I. Boustani, *Phys. Rev. B: Condens. Matter*, 1997, **55**, 16426–16438.
- 4 J. E. Fowler and J. M. Ugalde, *J. Phys. Chem. A*, 2000, **104**, 397–403.
- 5 J. I. Aihara, H. Kanno and T. Ishida, *J. Am. Chem. Soc.*, 2005, **127**, 13324–13330.
- 6 E. Oger, N. R. M. Crawford, R. Kelting, P. Weis, M. M. Kappes and R. Ahlrichs, *Angew. Chem., Int. Ed.*, 2007, **46**, 8503–8506.
- 7 H. J. Zhai, A. N. Alexandrova, K. A. Birch, A. I. Boldyrev and L. S. Wang, *Angew. Chem., Int. Ed.*, 2003, **42**, 6004–6008.
- 8 H. J. Zhai, B. Kiran, J. Li and L. S. Wang, *Nat. Mater.*, 2003, **2**, 827–833.
- 9 B. Kiran, S. Bulusu, H. J. Zhai, S. Yoo, X. C. Zeng and L. S. Wang, *Proc. Natl. Acad. Sci. U. S. A.*, 2005, **102**, 961–964.
- 10 A. P. Sergeeva, D. Yu. Zubarev, H. J. Zhai, A. I. Boldyrev and L. S. Wang, *J. Am. Chem. Soc.*, 2008, **130**, 7244–7246.
- 11 W. Huang, A. P. Sergeeva, H. J. Zhai, B. B. Averkiev, L. S. Wang and A. I. Boldyrev, *Nat. Chem.*, 2010, **2**, 202–206.
- 12 A. P. Sergeeva, B. B. Averkiev, H. J. Zhai, A. I. Boldyrev and L. S. Wang, *J. Chem. Phys.*, 2011, **134**, 224304 (11 pages).

- 13 A. P. Sergeeva, Z. A. Piazza, C. Romanescu, W. L. Li, A. I. Boldyrev and L. S. Wang, *J. Am. Chem. Soc.*, 2012, **134**, 18065–18073.
- 14 T. B. Tai, A. Ceulemans and M. T. Nguyen, *Chem.–Eur. J.*, 2012, **18**, 4510–4512.
- 15 H. Bai and S. D. Li, *J. Cluster Sci.*, 2011, **22**, 525–535.
- 16 J. K. Olson and A. I. Boldyrev, *J. Phys. Chem. A*, 2013, **117**, 1614–1620.
- 17 A. N. Alexandrova, E. Koyle and A. I. Boldyrev, *J. Mol. Model.*, 2006, **12**, 569–576.
- 18 N. G. Szwacki, V. Weber and C. J. Tymczak, *Nanoscale Res. Lett.*, 2009, **4**, 1085–1089.
- 19 Q. Chen, H. Bai, J. C. Guo, C. Q. Miao and S. D. Li, *Phys. Chem. Chem. Phys.*, 2011, **13**, 20620–20626.
- 20 D. Z. Li, H. G. Lu and S. D. Li, *J. Mol. Model.*, 2012, **18**, 3161–3167.
- 21 Q. Chen and S. D. Li, *J. Cluster Sci.*, 2011, **22**, 513–523.
- 22 H. Bai, Q. Chen, Y. F. Zhao, Y. B. Wu, H. G. Lu, J. Li and S. D. Li, *J. Mol. Model.*, 2013, **19**, 1195–1204.
- 23 W. J. Tian, H. Bai, H. G. Lu, Y. B. Wu and S. D. Li, *J. Cluster Sci.*, 2013, DOI: 10.1007/s10876-013-0603-2.
- 24 D. Z. Li, Q. Chen, Y. B. Wu, H. G. Lu and S. D. Li, *Phys. Chem. Chem. Phys.*, 2012, **14**, 14769–14774.
- 25 W. L. Li, C. Romanescu, T. Jian and L. S. Wang, *J. Am. Chem. Soc.*, 2012, **134**, 13228–13231.
- 26 D. Yu. Zubarev and A. I. Boldyrev, *Phys. Chem. Chem. Phys.*, 2008, **10**, 5207–5217.
- 27 B. Silvi and A. Savin, *Nature*, 1994, **371**, 683–686.
- 28 A. D. Becke and K. E. Edgecombe, *J. Chem. Phys.*, 1990, **92**, 5397–5403.
- 29 J. C. Santos, J. Andres, A. Aizman and P. Fuentealba, *J. Chem. Theory Comput.*, 2005, **1**, 83–86.
- 30 P. v. R. Schleyer, C. Maerker, A. Dransfeld, H. Jiao and N. J. R. E. Hommes, *J. Am. Chem. Soc.*, 1996, **118**, 6317–6318.
- 31 J. P. Perdew, K. Burke and M. Ernzerhof, *Phys. Rev. Lett.*, 1996, **77**, 3865–3868.
- 32 J. P. Perdew, K. Burke and M. Ernzerhof, *Phys. Rev. Lett.*, 1997, **78**, 1396.
- 33 C. Adamo and V. Barone, *J. Chem. Phys.*, 1999, **110**, 6158–6170.
- 34 A. D. Becke, *J. Chem. Phys.*, 1993, **98**, 5648–5652.
- 35 C. Lee, W. Yang and R. G. Parr, *Phys. Rev. B*, 1988, **37**, 785–789.
- 36 M. J. Frisch, G. W. Trucks, H. B. Schlegel and G. E. Scuseria, *et al.*, *Gaussian 09, revision A.1*, Gaussian, Inc., Wallingford, CT, 2009.
- 37 J. Cizek, *Adv. Chem. Phys.*, 1969, **14**, 35–89.
- 38 G. E. Scuseria and H. F. Schaefer, *J. Chem. Phys.*, 1989, **90**, 3700–3703.
- 39 R. J. Bartlett and M. Musial, *Rev. Mod. Phys.*, 2007, **79**, 291–352.
- 40 D. J. Wales and J. P. K. Doye, *J. Phys. Chem. A*, 1997, **101**, 5111–5116.
- 41 U. Varetto, *MOLEKEL, version 5.4*, Swiss National Supercomputing Centre, Lugano, Switzerland.
- 42 All calculations of the infinite double-chain boron nanoribbon were implemented in VASP.5.2 (ref. 43) with the projector augmented wave (PAW) (ref. 44) pseudopotential method. The plane-wave cutoff and k -point mesh were set to 500 eV and $39 \times 1 \times 1$, respectively. The PBE exchange–correlation functional was employed in the geometric optimization and band structure calculation.
- 43 G. Kresse and J. Furthmuller, *Phys. Rev. B: Condens. Matter*, 1996, **54**, 11169–11186.
- 44 G. Kresse and D. Joubert, *Phys. Rev. B: Condens. Matter Mater. Phys.*, 1999, **59**, 1758–1775.
- 45 H. Tang and S. Ismail-Beigi, *Phys. Rev. Lett.*, 2007, **99**, 115501 (4 pages).
- 46 W. A. de Heer, *Rev. Mod. Phys.*, 1993, **65**, 611–676.
- 47 Each sp-hybridized periphery B atom in the DC nanoribbon structures contributes one electron (either $2p_y$ or $2p_z$; perpendicular to the B chain direction x) to form the delocalized π or σ CMOs, whereas the two sp^2 -hybridized corner B atoms are each terminated by one H atom.
- 48 E. S. Penev, S. Bhowmick, A. Sadrzadeh and B. I. Yakobson, *Nano Lett.*, 2012, **12**, 2441–2445.
- 49 X. J. Wu, J. Dai, Y. Zhao, Z. W. Zhuo, J. L. Yang and X. C. Zeng, *ACS Nano*, 2012, **6**, 7443–7453.
- 50 H. G. Lu, Y. W. Mu, H. Bai, Q. Chen and S. D. Li, *J. Chem. Phys.*, 2013, **138**, 024701 (4 pages).
- 51 N. G. Szwacki, A. Sadrzadeh and B. I. Yakobson, *Phys. Rev. Lett.*, 2007, **98**, 166804 (4 pages).
- 52 A. K. Singh, A. Sadrzadeh and B. I. Yakobson, *Nano Lett.*, 2008, **8**, 1314–1317.